Biopolymer-enhanced delivery of reactive sulfide reagents for in-situ mercury remediation of heterogeneous contaminated soils

Dorian Davarzani, Zeinab Derikvand, Stéphanie Betelu, Stéfan Colombano, Marcio Nascimento, Ioannis Ignatiadis, Daniel Hubé

Science of the Total Environment 949 (2024) 174901

Contents lists available at ScienceDirect

Science of the Total Environment

journal homepage: www.elsevier.com/locate/scitotenv

Biopolymer-enhanced delivery of reactive sulfide reagents for in-situ mercury remediation of heterogeneous contaminated soils

Dorian Davarzani [a,*], Zeinab Derikvand [a,b], Stéphanie Betelu [a], Stéfan Colombano [a], Marcio Nascimento [a], Ioannis Ignatiadis [a], Daniel Hubé [a]

[a] BRGM (French Géologique Survey), 3 Avenue Claude Guillemin, 45100 Orléans, France
[b] University of Rennes, CNRS, Géosciences Rennes, UMR 6118 Rennes, France

HIGHLIGHTS

- Xanthan gum boosts pyrite microparticle stability for effective in-situ mercury remediation.
- Pyrite microparticles and sulfide reagents reduce xanthan polymer viscosity, retaining shear-thinning.
- Synergistic xanthate floating and xanthan gum shear-thinning enhance pyrite delivery in porous media.
- Xanthan gum achieves stable displacement front, enhancing pyrite powder delivery in heterogeneous media.
- Xanthan polymer, sulfide reagents, and pyrite microparticles synergize for novel, efficient environmental remediation.

GRAPHICAL ABSTRACT

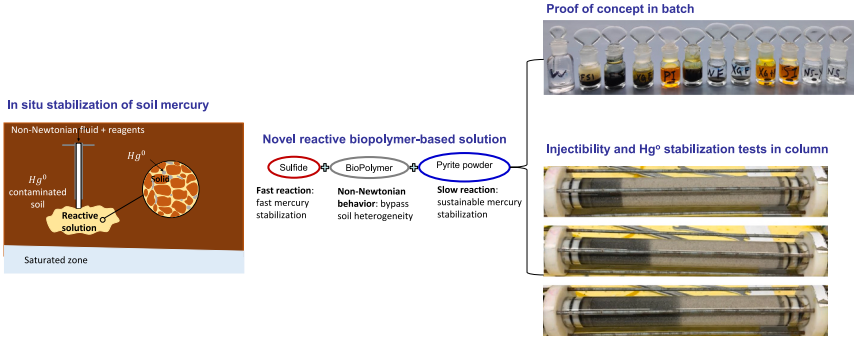

ARTICLE INFO

Keywords:
Contaminated soils
Mercury
Non-Newtonian fluids
Remediation
Stabilization

ABSTRACT

Mercury pollution from natural and anthropogenic sources demands effective remediation. This study focuses on optimizing a chemical stabilization approach using sulfur-containing compounds to create stable mercury sulfide (HgS) and immobilize elemental mercury in polluted soils. We propose using xanthan gum biopolymer to enhance the in-situ delivery of sulfide microparticles, overcoming soil heterogeneities due to its non-Newtonian behavior. Stability tests indicated that increased biopolymer concentration enhances particle stability due to the viscous and shear-thinning behavior of the polymer solutions. Various combinations (12 solutions) of xanthan polymer, pyrite microparticles, and sulfide-containing reagents were tested in batch experiments. Pyrite microparticles slightly reduced the xanthan solution's viscosity while retaining its non-Newtonian character. All solutions effectively transformed liquid mercury droplets into cinnabar, demonstrating successful mercury stabilization. Notably, solutions containing PIAX and SIPX, xanthate organosulfur compounds, significantly reduced the dissolved concentration of elemental mercury. Column experiments demonstrated xanthan gum's superior performance for in-situ injection of pyrite microparticles and sulfide mixtures into the soil compared to conventional water injection. At a polymer concentration of 4 g/L, a stable displacement front and an 88 % recovery of the initially injected particle-suspension density were achieved. The combined effects of xanthate's floating behavior and xanthan gum's shear-thinning nature substantially enhanced the delivery of pyrite microparticles in porous media for soil mercury remediation. This combination reduced the aqueous elemental mercury

* Corresponding author.
E-mail address: d.davarzani@brgm.fr (D. Davarzani).

https://doi.org/10.1016/j.scitotenv.2024.174901
Received 30 December 2023; Received in revised form 15 July 2024; Accepted 18 July 2024
Available online 20 July 2024

concentration in artificially polluted sand by up to 97 %, particularly with the xanthate organosulfur compound, PIAX. Xanthate has a higher potential to react with elemental mercury to form cinnabar compared to sodium thiosulfate. Additionally, the pyrite microparticles, rendered hydrophobic in xanthate solutions, integrated into the mercury droplets, forming a black paste. This study introduces a promising approach for efficient elemental mercury stabilization in contaminated soils by integrating biopolymers, reactive soluble compounds, and pyrite microparticles for sustainable decontamination.

1. Introduction

Soil contamination with mercury (Hg) is a major environmental issue with significant impacts on human health and the ecosystem. Mercury, a toxic heavy metal, can linger in the environment for decades and pose harm to human health through both the food chain and direct contact. The production and use of mercury, dating back to the 19th century, has led to a major issue with mercury pollution. Methylmercury ($[CH_3Hg]^+$), a toxic form of mercury, can easily enter the food chain and pose a risk to human health with research indicating a greater biological accumulation and a larger magnification in the food chain (Abeysinghe et al., 2017; S. Liu et al., 2021b). Human activities following the industrial era have contributed to the elevated levels of Hg in soil and sediment, with 3–10 times increase (S. Liu et al., 2021b).

The primary sources of soil contamination are usually attributed to mining operations and industrial production (Ukaogo et al., 2020). A recent study conducted across China revealed that soil contamination with mercury was a widespread issue, with 1.6 % of the surveyed sites exceeding the regulatory limit set by the country's Ministry of Land and Resources (MLR) and Ministry of Environmental Protection (MEP) (Gong et al., 2019). In response, the search for effective ways to remediate soil contaminated with mercury has gained considerable attention. Previous attempts have focused on various methods, including physical (Sierra et al., 2011), chemical (Ying and Zhou, 2005), and biological approaches (Mahbub et al., 2017). Physical methods include the excavation and removal of contaminated soil, while chemical methods involve the use of various reagents such as chelating agents, acids, and bases (Li et al., 2019). Biological approaches rely on microorganisms to remove mercury from soil through biomethylation.

The chemical stabilization approach uses sulfur-containing compounds to react with elemental mercury (Hg^0) in contaminated soil to form mercury sulfide (HgS) which is a stable and insoluble compound (Hagemann, 2009; Rodríguez et al., 2012). However, it can be challenging to deliver in situ reactive compounds using traditional Newtonian fluids in heterogeneous soils.

Moreover, the use of polymers offers several advantages in the remediation of Hg-contaminated soils. Polymers are non-toxic, biodegradable, and can effectively bind to mercury ions, preventing their spread and bioavailability (Zhao et al., 2023). In addition, polymers can be easily modified to improve their mercury binding capacity and can be combined with other materials, such as nanoparticles, to enhance the remediation process (Wang et al., 2020).

In addition to the use of polymers for Hg remediation, researchers have also investigated the efficacy of pyrite and synthetic FeS for Hg removal. Pyrite, a naturally occurring mineral, has been shown to be effective for remediating low-concentration Hg-contaminated soils, while synthetic FeS exhibits a superior performance for treating high-concentration Hg-containing wastewater (Han et al., 2020; Skyllberg et al., 2021; Sun et al., 2017). Bower et al. (2008) investigated the influence of pH, reaction time, and Hg(II) concentration on pyrite's ability to sorb Hg(II) (Bower et al., 2008). Their batch sorption studies revealed that higher pH and longer reaction times increased Hg(II) removal. They suggested that pyrite has the potential to serve as an effective reactive barrier for Hg(II) remediation and that optimizing conditions, such as pH and oxygen content, could further enhance its effectiveness. They used two 1-cm diameter glass tubes were packed with 6.30 g of pure quartz sand, one with and one without a pyrite barrier. The barrier column had 0.25 g of washed pyrite mixed with 0.75 g of quartz sand, evenly distributed at the top. The presence of a thin reactive barrier of pyrite in the column experiments greatly slowed the effluent of Hg(II), delaying breakthrough by approximately 15 times (Bower et al., 2008). Duan et al. (2016) investigated the synthesis of nanoscale pyrite particles for mercury removal and found that it achieved high removal rates (90 %) within 5 min and complete removal after 12 h (Duan et al., 2016). However, the presence of salts reduced the removal efficiency. This study highlights the potential of nanoscale pyrite as a highly efficient adsorbent for mercury removal. Sun et al. (2017) conducted a comparative analysis of natural pyrite and synthetic FeS for Hg(II) adsorption in aqueous systems (Sun et al., 2017). Their findings revealed that synthetic FeS exhibited a remarkable advantage, boasting a maximum sorption capacity of 769.2 mg/g compared to pyrite's 9.9 mg/g. This substantial difference was attributed to the larger surface area of synthetic FeS, providing ample sites for Hg(II) attachment. They further highlighted synthetic FeS's remarkable tolerance to pH variations, chloride ions, and coexisting cations, rendering it a promising sorbent for treating high-concentration Hg(II)-containing wastewater (<20 mg/L). In contrast, pyrite, despite its lower sorption capacity, stands out as an effective long-term adsorbent for immobilizing wastewater with lower Hg(II) concentrations (<1 mg/L) due to its economic feasibility and abundance.

Beyond the use of pyrite, researchers have also explored the efficacy of alternative methods for mercury removal, including sodium thiosulfate ($Na_2S_2O_3$) and sodium sulfide (Na_2S). Ray and Selvakumar used a synergistic combination of hydrogen peroxide (H_2O_2), sodium thiosulfate ($Na_2S_2O_3$), and sodium sulfide (Na_2S) to remediate mercury-contaminated soil, achieving a remarkable mercury removal rate of 88.6 % (Ray and Selvakumar, 2000). Their study demonstrated the effectiveness of this approach in reducing the final mercury concentration in the soil from an initial concentration of 2100 mg/kg to 270 mg/kg. Chen and Zhang (2012) later investigated the application of $Na_2S_2O_3$ solution for mercury removal from soil with an initial concentration of 108.76 mg/kg, achieving a removal rate of approximately 65 % (Chen and Zhang, 2012). Their findings further reinforced the potential of sodium thiosulfate as a mercury remediation agent.

The combination of polymers and nanoparticles can improve the overall efficiency and effectiveness of the remediation process and reduce the cost associated with traditional remediation methods (Tungittiplakorn et al., 2005). Liu et al. (W. Liu et al., 2021a) investigated the use of xanthan gum (XG) to stabilize reduced graphene oxide-based nanoscale zero-valent iron (nZVI/rGO) for in-situ remediation of a Cr(VI)-contaminated aquifer. They demonstrated that XG-nZVI/rGO effectively formed an in-situ reaction zone, successfully reducing Cr (VI) downstream for a duration of 108 h. Notably, their remediation approach had minimal impact on the aquifer's pH and produced a limited quantity of Fe^{2+}, ensuring a reduced risk to environmental microorganisms. While the effectiveness of XG in absorbing heavy metals such as Cd, Cu, Pb, and Zn from soil is well-documented (Han et al., 2022; Ko et al., 2022), its application in soil remediation for Hg^0 contamination remains underexplored. In contrast, the capacity of FeS and FeS_2 to form complexes with Hg and reduce its mobility is established (Lyu et al., 2016).

Significantly, our study marks the first exploration of the synergistic effects resulting from the combination of a biopolymer (xanthane), the micro-particle of pyrite and reactive sulfide reagents. Additionally, the

mercury fixation ability of pyrite has been predominantly studied in aqueous solutions (Gong et al., 2019). Therefore, investigating the potential of pyrite for remediating mercury-contaminated soil under hydrodynamic conditions is of significant interest. These reactive sulfide reagents encompass sodium sulfide, sodium thiosulfate, and particularly, two novel xanthate formulations (potassium isopropyl xanthate and sodium isobutyl xanthate). Xanthates are widely used as flotation agents in the mining industry for the extraction of metals, including gold. Their floating behavior is primarily due to their ability to act as collectors in the froth flotation process. Particularly, the adsorption of xanthates imparts hydrophobic characteristics to the metal particles. The xanthate forms a monolayer on the particle surface, making it water-repellent (Rao and Finch, 2003). The conversion of particles to a hydrophobic state significantly improves their ability to float in the aqueous phase (Peng et al., 2018).

A better understanding of the combined use of these materials could lead to improved remediation strategies for mercury contaminated soils, reducing the risk of Hg leaching into the environment and potentially reducing the costs associated with Hg remediation. In this study, we aim to investigate the synergistic effects of XG polymer and iron sulfides in removing Hg from soil. We show how injecting biopolymer can improve the delivery of sulfide micro-particles and reagents. The main objective is therefore to develop a biopolymer and sulfide-based solution to stabilize the elemental mercury but also to study the feasibility of injecting in situ such a solution into polluted soil. To achieve this goal, several experiments have been conducted including a stability study, characterization of polymer, transport study in a porous medium, and investigation of polymer concentration effects. The results of these experiments have led to the development of a method to reduce mercury saturation in contaminated soils using non-Newtonian liquids loaded with sulfur.

2. Materials and methods

2.1. Materials

2.1.1. Biopolymer

Xanthan gum, with the chemical formulas of $C_{35}H_{49}O_{29}$ was provided from Sigma-Aldrich for use in our experiments. This biopolymer, commonly known as XG, is a high-molecular-weight polysaccharide derived from the fermentation of sugars by the bacterium *Xanthomonas campestris* (Shabir et al., 2023). XG exhibits exceptional rheology, offering a unique combination of shear-thinning and shear-thickening behavior. Its non-Newtonian properties make it an ideal carrier fluid for in-situ mercury remediation, particularly in heterogeneous soil environments. XG is a white or off-white powder, non-toxic, odorless, and biodegradable, and it readily dissolves in both hot and cold water. Its solubility in cold water makes it a practical choice for in-situ remediation, as it can be injected directly into the soil without the need for heating or pre-treatment. XG is also insoluble in alcohol, further enhancing its suitability for soil remediation applications. Its exceptional thickening and suspensive power enable the creation of highly viscous solutions that effectively maintain particle suspension in the presence of sulfide microparticles and reactive reagents. Furthermore, XG's viscosity is minimally affected by temperature variations, ensuring consistent delivery and performance across a range of soil temperatures.

2.1.2. Iron sulfides microparticles

Powdered sulfide minerals were utilized in the formulation of polymer solutions. Pyrite (FeS_2) with a 98.9 % purity, a particle size of 1–5 μm, and a density of 5.00 g/cm^3 was obtained from Nanochemazone (Canada). The concentration of FeS_2 in the experiments was established as 24 g/L, as recommended by the research performed by Bower et al. (Bower et al., 2008).

2.1.3. Sulfide compounds reagents

In this study, we have tested potassium isopropyl xanthate or PIAX ($(CH_3)_2CHOCS_2K$) and sodium isobutyl xanthate or SIPX ($(CH_3)_2CHCH_2OCS_2Na$). Xanthates, also known as dithiocarbonates, are compounds derived from the salts and esters of xanthic acid. The term "xanthic acids" encompasses a group of organosulfur compounds with the general formula ROC(=S)SH, effectively making them O–esters of dithiocarbonic acid. Deprotonation results in the formation of the xanthate anion with the general formula ROC(=S)S.

Furthermore, we examined the effectiveness of sodium thiosulfate ($Na_2S_2O_3$) and sodium sulfide (Na_2S) as chemical agents for stabilizing elemental mercury. Notably, xanthates (PIAX and SIPX) have not previously been employed for this purpose. In contrast, it is established that sodium thiosulfate and sodium sulfide can facilitate the precipitation of elemental mercury in the form of cinnabar. To ensure the stability of our solutions, it is crucial to control and maintain the pH of the prepared solution within the optimal range of 8 to 12. To achieve this pH range, we employed two buffer solutions, namely K_2CO_3 and $KHCO_3$, to adjust the pH of solutions to approximately 10.

2.1.4. Gas and water

Gases of CO_2 (purity 99.7 %) and N_2 (purity 99.98 %) were supplied by Air Liquide and utilized in our experimental procedures. CO_2 was employed to prevent formation of air bubbles during the column soaking process. Meanwhile, N_2 served to prevent the agglomeration of microparticles in the polymer solution and shielded against the oxidation of pyrite microparticles during the preparation process. Throughout the study, we exclusively used deionized water sourced from a Millipore purification system (Elix Advantage range).

2.1.5. Siliceous sand for porous medium construction

To establish authentic and permeable soil conditions, we employed a dry, highly siliceous sand obtained from SIBELCO as the porous medium for this research. The particle size range for this study was restricted to 0.7 to 1 mm to ensure optimal injectability of microparticles with the polymer solutions. This was achieved by carefully sieving the sand to meet the specified size criteria. Subsequently, a thorough washing process was conducted to eliminate any impurities and ensure the purity of the porous medium. Finally, the sand was subjected to drying in an oven at 100 °C for 15 h to remove residual moisture and ensure consistent flow properties of the polymer solutions.

2.2. Experimental setups and procedures

2.2.1. Preparation of solutions

All polymer-based solutions were prepared using deionized water. A one-liter suction flask was filled with deionized water and placed on a magnetic stirrer to facilitate thorough mixing. The water was then connected to a vacuum pump to efficiently remove any air bubbles, ensuring a homogeneous solution. This degassing process was conducted for 30 min at a rotation speed of 500 rpm to ensure thorough removal of air pockets.

Following degassing, the deionized water was transferred to a beaker where the polymer solution would be prepared. The mixing of the solutions was performed using an overhead stirrer (IKA RW14) at a rotation speed ranging from 200 to 500 rpm for a duration of 1 to 4 h. For the batch tests, a series of combinations involving sulfide compounds, polymers (XG), and buffer solutions were prepared to evaluate their effectiveness in mercury stabilization. Table 1 provides a comprehensive list of all the solutions utilized in the batch experiments.

The preparation of polymer-based solutions (stock or mother solutions) on pyrite and/or sulfide compounds was conducted following a sequential approach. Firstly, all water-soluble components were prepared, followed by the addition of buffer solutions, and subsequently, the polymers were introduced. However, in cases involving the incorporation of a water-insoluble solution (e.g., pyrite micro-particles), the

Table 1
Different formulations of polymer solutions with sulfide components (concentration is in g/L).

Number	1	2	3	4	5	6	7	8	9	10	11	12	13
Solutions	W.F	XG.F	SI	PI	XG.SI	XG.PI	XG.SI.F	XG.PI.F	NS	XG.NS	XG.NS.F	XG.TS.F	XG
XG	–	4	–	–	4	4	4	4	–	4	4	4	4
FeS_2	24	24	–	–	–	–	24	24	–	–	24	24	–
SIPX	–	–	100	–	100	–	100	–	–	–	–	–	–
PIAX	–	–	–	100	–	100	–	100	–	–	–	–	–
K_2CO_3	–	–	38.12	29.14	38.12	29.14	38.12	29.14	38.12	38.12	38.12	38.12	–
$KHCO_3$	–	–	4.36	29.95	4.36	29.95	4.36	29.95	4.36	4.36	4.36	4.36	–
Na_2S	–	–	–	–	–	–	–	–	20	20	20	–	–
$Na_2S_2O_3$	–	–	–	–	–	–	–	–	–	–	–	20	–

XG: xanthan gum; W: Deionized water; FeS_2 (F): pyrite powder; SIPX (SI): Sodium isopropyl xanthate; PIAX (PI): Potassium isoamyl xanthate; K_2CO_3 and $KHCO_3$: buffers; Na_2S (NS): Sodium sulfide; $Na_2S_2O_3$ (TS): sodium thiosulfate.

particles were introduced into the aqueous phase prior to the polymer powder addition. To prepare the polymer solution, hydration of iron sulfide in water was initiated at 200 rpm for 15 min, followed by the subsequent addition of the polymer powder and mixing at 500 rpm for 3 h. Regarding column injection, only formulations 1, 2, 8, and 12 were utilized. The concentrations of the sulfide solutions were determined empirically based on their solubility in water. The stability of the solutions was assessed using graduated cylinders, and all experiments were conducted in a temperature-controlled room at 20 °C.

2.2.2. Batch experiments and analytical method

To assess the efficacy of polymer-based solutions in stabilizing elemental mercury (Hg^0) and promoting its transformation to cinnabar, a series of batch experiments were conducted. In this study, all solutions listed in Table 1 were prepared, and all were spiked with a known dissolved concentration of mercury at 100 ng/L. This controlled spiking allowed for the systematic investigation of the solutions' ability to stabilize and facilitate the conversion of elemental mercury. The concentration of mercury before and after spiking were analyzed. By systematically spiking the solutions and tracking the transformation kinetics, we sought to provide valuable insights into the potential of polymer-based solutions for stabilizing elemental mercury and facilitating its conversion to cinnabar, contributing to the understanding of mercury remediation strategies.

Employing the Analytik Jena Mercur DUO PLUS atomic fluorescence spectrometer, we developed a comprehensive analytical protocol for accurate and reliable quantification of mercury concentrations in the stock solutions. This advanced instrument features a cold vapor generator, an atomic fluorescence detector, and a signal processing system, complemented by a 54-position sample changer (AS-FD sampler). The analytical procedure involves a series of sequential steps to effectively convert mercury species into a form suitable for quantification.

Initially, samples undergo thorough mineralization with a bromide/bromate mixture in hydrochloric acid. This step ensures the complete transformation of all mercury species into the divalent state (II). Subsequently, residual bromine is removed using ascorbic acid to prevent interference with the subsequent mercury quantification process. Next, mercury (II) is further reduced to elemental mercury (Hg^0), the most stable and easily quantifiable form, using stannous chloride. The released elemental mercury is then transported into the atomic fluorescence detector as cold vapors via a carrier gas (argon). Within the detector, the monoatomic vapor state of mercury is excited by ultraviolet light at a wavelength of 254 nm, and the resulting fluorescence signal is measured. This signal is proportional to the concentration of mercury in the sample, enabling accurate quantification. The analytical workflow outlined here demonstrates the robustness, sensitivity, and precision of the mercur DUO PLUS system for mercury analysis, making it a valuable tool for investigating mercury contamination in complex matrices.

Then, all reactions involving the interaction of liquid pure mercury with polymer solutions were carried out within test tubes. Within these test tubes, we monitored the ability of polymer solutions to stabilize mercury as well as its conversion into cinnabar. Each test tube was comprised of a glass sample approximately 40 mm in length and possessed an inner diameter of 15 mm. A glass stopper was used to prevent the loss of Hg^0 due to volatilization from the glass tube.

To evaluate the effectiveness of the prepared solutions in stabilizing elemental mercury (Hg^0), we introduced approximately 0.4 g of liquid Hg^0 to the bottom of each test tube. Subsequently, 2.7 mL of the prepared solutions (refer to Table 1 for details) were added to the test tubes without shaking. Shaking the tubes can dislodge the cinnabar formed at the interface of the mercury, potentially altering the results. The shaking condition does not correspond to the in situ real case. The surface condition and any color changes in the mercury were visually examined after its exposure to the sulfide biopolymer-based solutions. Additionally, we monitored any alterations in the color of the solutions due to chemical interactions. The precise quantities used were measured using a precision balance (Fisherbrand™ Precision Balances) with an accuracy of ±0.001 g and a volumetric pipette in order to ensure method accuracy. To mitigate contamination resulting from the volatilization of Hg^0 during sample preparation, all tests were conducted in a dedicated room with appropriate facilities and within a fume hood.

2.2.3. 1D column for flooding experiments

The behavior of polymer solutions in porous media and the influence of polymer concentration on solution vectorization were assessed using a glass column filled with a clean porous medium, as depicted in Fig. 1. Subsequently, the stabilization of elemental mercury was performed by injecting the most promising solutions into Hg^0-doped porous media. The column measured 30 cm in length and 4 cm in inner diameter, providing a controlled environment to assess the flow behavior of the solutions. The porous medium was secured in place using metal grids with a mesh size of 250 μm, ensuring uniform distribution of the solutions within the column.

To monitor the progress of the flooding experiments, a differential pressure sensor (KELLER PR33X pressure transducer) was employed to measure the pressure drop across the porous medium. An electronic

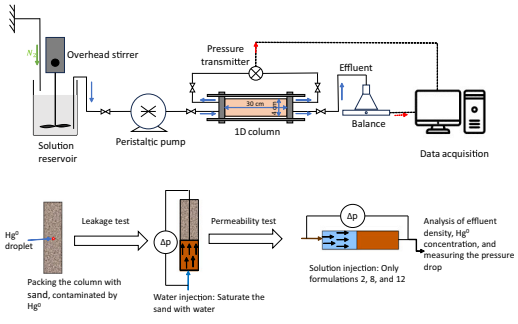

Fig. 1. An illustration of a) the setup and b) experimental protocol used for flooding experiments.

balance (OHAUS, model STX 6201) was used to track the weight change of the column, providing information about the amount of solution injected. Data acquisition and analysis were conducted using control series 3.0 software, enabling precise tracking of the displacement process. An Ismatec® Reglo ICC digital peristaltic pump (accuracy ±1 %) was employed to inject the solution from a reservoir into the packed column, maintaining a constant flow rate during the flooding experiments.. The Masterflex® PTFE tubing with individual channel control ensured efficient delivery of the polymer solutions through the column. To maintain the homogeneity of the injected solutions and prevent the precipitation of microparticles, a mechanical rod stirrer was integrated into the reservoir containing the solution. A schematic view of the displacement test setup is illustrated in Fig. 1.

The dry sand was carefully loaded into the column vertically to ensure proper packing. The sand was compacted every 5 cm using a rod to mitigate local heterogeneity and prevent preferential pathways. In the Hg^0-doped column, a 4-g mercury droplet was placed in the column center. Preventing soil and mercury mixing enhances experiment repeatability. A leak test was conducted on the column by applying 1 bar of CO_2 gas pressure, and leaks were detected using foam soap. Subsequently, the column was flushed with CO_2 at a flow rate of 5 mL/min for 45 min to achieve fully water saturation and avoid air bubble by dissolving the CO_2 gas.

Deionized water was introduced from the bottom of the column at a flow rate of 1 mL/min to attain fully water saturation by removing gas gradually from the top of the column. The column's weight before and after water saturation was measured to determine the pore volume (PV = 143 mL) and porosity (0.38). Permeability was calculated by measuring pressure changes along the column for different flow rates, applying Darcy's law. Table 2 provides the properties of the sand utilized, including diameter (mm), pore volume (PV), porosity (%), permeability (darcy), and equivalent radius, r_{eq} (μm).

Finally, the solutions were horizontally injected into the columns at a flow rate of 3.48 mL/min. Three series of experiments were performed to achieve different objectives: i) injection of 3 pore volumes (PV) of water and biopolymer (2 g/L and 4 g/L) charged with pyrite microparticles to study the effect of the biopolymer and its concentration on particle delivery and fluid front propagation in porous media, ii) injection of 3 PV of the most promising biopolymer-based solutions to evaluate their efficiency in delivering the pyrite microparticles, iii) injection of 3 PV of water followed by 1 PV immediately and 1 PV after 3 days of the selected solutions into the Hg^0-doped column to study their efficiency in stabilizing elemental mercury.

During the experiments, the pressure drop was continuously monitored. The effluents were collected, and their density was measured using a 5 mL pycnometer. For the Hg^0-doped experiments, the effluents were collected after every 1 PV of solution injection in 7 mL polyethylene terephthalate tubes with stoppers for mercury concentration analysis.

2.2.4. Rheological behavior of solutions

All solutions were tested using a Haake Mars 60 Thermofisher rheometer (min. torque rotation 0.02 μN.m, torque resolution 0.1 nN.m) with cone-plate geometry (C60/1°/Ti and TMP60). 1–2 mL of solution was placed in the shear gap of 0.054 mm, and the shear rate was recorded over time with corresponding stress. The shear stress was adjusted between 0.01 and 100 s^{-1} with a maximum measurement time of 60 s. The results were verified with three tests of each polymer solution to ensure accuracy.

Table 2
Physical characteristics of porous medium.

Porous medium	Diameter, mm	PV, mL	Porosity, %	Permeability, darcy	r_{eq}, μm
Dry siliceous sand	0.7–1.0	143.12 ± 1.31	37.98 ± 0.35	247.3 ± 1.0	72.17 ± 0.29

2.2.5. Particle stability analyses of the polymer-based solutions

Stability assessments of polymer solutions were carried out within graduated cylinders. Initially, the stability of pure polymer solutions was examined to establish a baseline for comparison. Subsequently, pyrite microparticles (FeS_2) were added to the solutions to assess the influence of particle presence on stability. The experimental setup consisted of graduated glass cylinders with a length of 300 mm and an inner diameter of 40 mm. To monitor the stability of the pyrite particle suspensions, the height of the suspensions was measured continuously at regular 10-min intervals. This continuous monitoring allowed for the observation of any changes in particle sedimentation or solution homogeneity.

3. Results and discussions

3.1. Effect of polymer concentration on particle stabilization

Particle stability experiments were conducted to evaluate the stability of polymer solutions in the presence of FeS_2. The suspension volumes of the solutions were monitored over time, and the impact of polymer concentration on particle stability was examined. Fig. 2 presents the temporal evolution of suspension volume for XG solutions with concentrations of 1 g/L, 2 g/L, and 4 g/L while maintaining a constant FeS_2 concentration of 24 g/L. As indicated in Fig. 2, the solution with 1 g/L XG experiences a gradual reduction in suspension volume over 160 min, starting from an initial volume of 250 mL. A significant decline occurs within the first 100 min, resulting in a final reduction in volume of approximately 60 mL. This reduction suggests substantial precipitation of FeS_2 microparticle and the formation of distinct liquid layers. A similar trend, with a smaller volume reduction, is observed with the addition of 2 g/L XG, resulting in a 34 % lower reduction compared to the 1 g/L XG solution. However, the pyrite microparticles remained fully stable in the xanthan solution at a concentration of 4 g/L. This implies that an increase in polymer concentration enhances particle stability in the solution. Therefore, 2 g/L and 4 g/L XG are selected as the optimum concentrations for further experiments, potentially indicating a saturation point where additional polymer does not significantly impact the stability of the suspension.

The stability of microparticles in viscous fluids, such as XG, is governed by a set of key factors. The heightened viscosity plays a crucial role in impeding the settling of microparticles, providing resistance against gravitational forces, particularly benefiting smaller particles. The shear-thinning behavior inherent in polymer solutions facilitates ease of handling without compromising stability. During shear stress, the fluid's viscosity decreases, allowing for convenient manipulation, and promptly reverts to a higher viscosity, ensuring sustained stability.

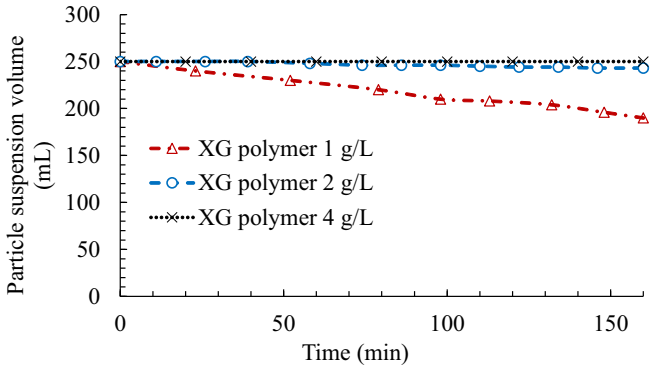

Fig. 2. Time-dependent particle stability of FeS_2 (24 g/L) in XG polymer solutions of different concentrations.

The increased viscosity and elasticity of the polymer solution collectively contribute to an improved suspension, fostering increased interparticle interactions. This interaction leads to the formation of a stable structure or network within the fluid, further enhancing microparticle dispersion. The elastic nature of the solution resists deformation, and its resilience against external forces, such as gravitational settling and turbulence, collectively maintains the dispersion of microparticles.

3.2. Rheological behavior of solutions

The rheological behavior of XG polymer solutions were analyzed by studying how their viscosity responded to changes in shear rates, as illustrated in Fig. 3. As depicted in Fig. 3a, XG solutions demonstrate shear-thinning characteristics, featuring elevated viscosity at low shear rates and decreased viscosity at high shear rates. The viscosity of XG displays a concentration-dependent pattern when doubling the concentration from 2 g/L to 4 g/L. Furthermore, there is an approximate rise in viscosity at shear rates of 0.1 and 1.0 1/s, with values increasing from 1.42 Pa.s to 7.94 Pa.s and 0.33 Pa.s to 1.31 Pa.s, respectively. This increase in viscosity with increasing polymer concentration can be attributed to the entanglement and interaction of polymer chains (Gao et al., 2018; Patel et al., 2020; Rezaeiakmal et al., 2022). As the concentration rises, there is a greater likelihood of polymer chain entanglements, resulting in increased resistance to flow and higher viscosity

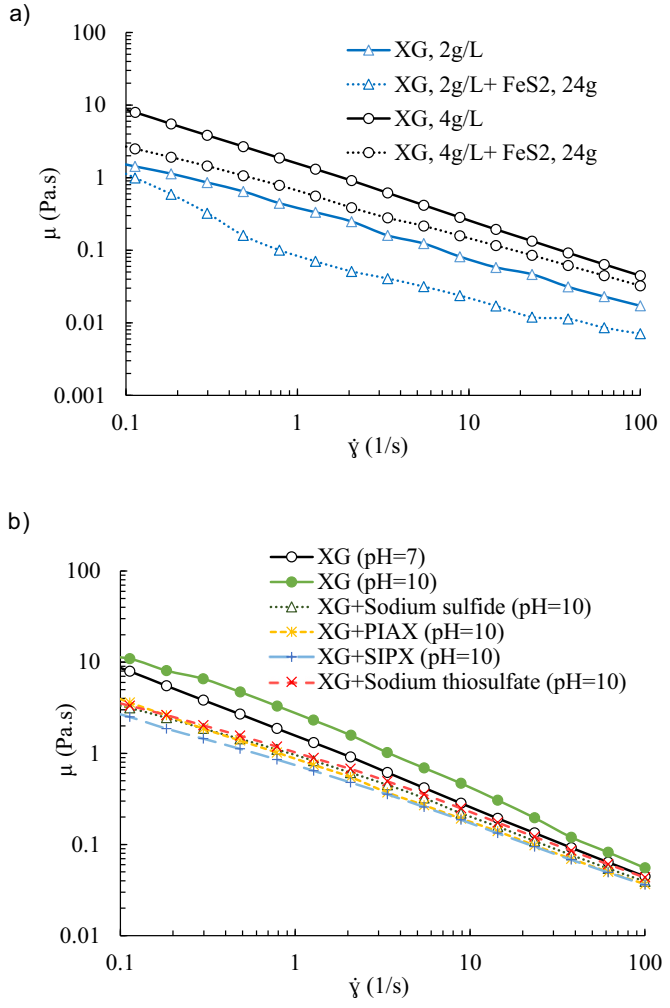

Fig. 3. Rheological behavior of a) the mixture of xanthan polymer of different concentration with and without pyrite powder and b) xanthan polymer (4 g/L) at pH 7 and 10, along with mixtures of xanthan polymer with different buffered sulfide reagents.

(Nsengiyumva and Alexandridis, 2022).

The addition of pyrite to both XG solutions, at concentrations of 2 g/L and 4 g/L, revealed a noteworthy trend in the viscosity-shear rate curves, as illustrated in Fig. 3a. This trend suggests a complex interplay between pyrite particles and the XG polymer solution's rheological behavior. Notably, the presence of pyrite exerted a dual effect on viscosity, resulting in an overall reduction in viscosity. This phenomenon can be attributed to the disruptive influence of pyrite particles on the polymer matrix, leading to a decreased resistance to flow (Liu et al., 2018). Intriguingly, the impact of pyrite was more pronounced in the lower concentration solution, where it accentuated the difference in viscosity between the two solutions, particularly at higher shear rates. This may imply concentration-dependent effects or enhanced pyrite-polymer interactions in the lower concentration solution. Importantly, it is worth mentioning that the introduction of microparticles did not result in any significant alteration in the non-Newtonian behavior of XG solutions. The rheological characteristics of the solutions remained consistent, indicating that the presence of pyrite microparticles did not induce substantial changes in the overall shear-thinning fluid nature.

Fig. 3b illustrates the rheological behavior of XG solutions at 4 g/L concentration at pH 7 and 10, along with when it is combined with different additives, including sodium sulfide, PIAX, sodium thiosulfate, and SIPX (see Table 4). Increasing the pH of the xanthan solution from 7 to 10 maximally increases the viscosity of the solution by a factor of 1.3 while maintaining its non-Newtonian rheological behavior. In this range of pH, the xanthan gum molecules are fully hydrated and interact strongly with water, resulting in a highly viscous solution. The viscosity tends to remain relatively stable and high within this pH range. However, these general trends can vary depending on the specific formulation and concentration of the xanthan gum solution, as well as the presence of other ions or additives in the solution (Nsengiyumva and Alexandridis, 2022). Moreover, all additives reduce the viscosity compared to the base XG solution keeping a good non-Newtonian behavior. Notably, the addition of SIPX results in a linear reduction, distinguishing it from the other additives, which exhibit similar trends to XG alone. At lower shear rates (below 1 1/s), the XG + PIAX solution exhibits significantly higher viscosity compared to other additive solutions. This demonstrates the unique impact of PIAX on the rheological properties of the polymer solution.

3.3. Mercury stabilization test in batch

The initial and post-spiking concentrations of Hg^0 in various reactive sulfide reagents were measured using the Analytik Jena Mercur DUO PLUS, and the results are presented in Table 3. Despite the complex composition of the solutions, the analyzer demonstrated its suitability for mercury quantification, as the Hg^0 concentrations in the initial solutions were within its measurable range, considering the low detection limit of 50 ng/L.

Upon spiking 100 ng/L of dissolved mercury into the solutions, all measured values remained below the analyzer's detection limit. Notably, it was observed that the addition of 100 ng/L of mercury to pure water and only polymer solution resulted in no significant change in mercury concentration. This intriguing observation underscores the stability of mercury in water and polymer under these conditions and further validates the precision and sensitivity of the analyzer. The lack of significant change in mercury concentration in pure water contrasts with the observed reductions in mercury concentration in the reactive sulfide reagents (Solutions 3–12). The higher concentrations observed in solutions containing water and polymer associated with pyrite powder (Solutions 1 and 2) may be attributed to the slow kinetics of the pyrite reaction with dissolved mercury and its limited reaction surface. In contrast, solutions in the form of liquid reagents exhibited rapid reactions, resulting in a substantial reduction in mercury concentration.

The results obtained from batch experiments demonstrate that the addition of polymer does not significantly hinder the reagents' ability to

Table 3
Initial and post-spiking Hg^0 concentrations in various reactive sulfide reagents measured using Analytik Jena Mercur DUO PLUS.

Solution number	1	2	3	4	5	6	7	8	9	10	11	12	13	Only water
Solution name	W.F	XG.F	SI	PI	XG.SI	XG.PI	XG.SI.F	XG.PI.F	NS	XG.NS	XG.NS.F	XG.TS.F	XG	W
Initial Hg^0 concentration (ng/L)	20 ± 1	4 ± 0	9 ± 3	2 ± 0	1 ± 0	3 ± 1	1 ± 0	2 ± 0	4 ± 2	9 ± 1	3 ± 2	2 ± 1	1 ± 1	1 ± 1
post-spiking Hg^0 concentration (ng/L)	42 ± 0	25 ± 0	13 ± 2	2 ± 0	9 ± 3	10 ± 1	4 ± 0	7 ± 0	5 ± 1	8 ± 1	6 ± 2	2 ± 1	94 ± 2	99 ± 4

stabilize dissolved mercury. This finding suggests that the polymer does not compete with the reagents for interaction with mercury, allowing for efficient stabilization. Overall, the results highlight the efficacy of the selected sulfide reagents for mercury stabilization, demonstrating their potential for practical application in environmental remediation scenarios.

Furthermore, the tube experiments involving the addition of mercury droplets into the mother solutions revealed a distinct color transformation in all proposed sulfide reagents, where the initial silvery-white appearance of mercury changed to shades of gold, dark gold, or black. This observed change in color indicates the conversion of mercury into cinnabar upon contact with the reagent. The pyrite microparticles, rendered hydrophobic in xanthate solutions (solutions 7 and 8), integrated into the mercury droplets, forming a black paste. However, the pyrite particles remained on the surface of the mercury droplets for other solutions. Due to the inherent complexity of our solutions, characterized by the presence of microparticles and polymers, attempts to quantitatively assess the cinnabar content proved challenging. Notably, the solution containing xanthate exhibited an orange color, while the addition of pyrite powder resulted in a complete blackening of the solution. Remarkably, we observed that pyrite microparticles remained in suspension within the xanthate solution even after more than one year. This prolonged suspension behavior suggests potential advantages for injecting pyrite microparticles into porous media, minimizing clogging and enhancing interactions with mercury droplets in soil. The floating behavior of xanthates is noteworthy, attributed to their ability to modify the surface properties of pyrite particles, rendering them hydrophobic (Wang and Eric Forssberg, 1991; Yang et al., 2018) and facilitating attachment to non-wetting droplets of mercury. This unique floating behavior underscores the versatility of xanthate-containing solutions and their potential applications in environmental remediation scenarios. No change in color was observed in the mercury droplet when in contact with either pure water or the polymer alone (solution 13).

3.4. Solutions injectability and mercury stabilization tests in 1D sand-packed column

3.4.1. Effect of xanthane biopolymer and its concentration on microparticle delivery

The injectability of the solution is one of the obstructions for field application. Fig. 4 provides a visual representation of column conditions following the injection of various solutions including water and biopolymer (xanthane) solution of 2 g/L and 4 g/L in combination of pyrite micro-particles at different pore volumes. Blank water injection shows particle accumulation downstream, stagnating front due to low water viscosity causing rapid particle settling. After the injection of 1 PV, the particle front remains stagnant due to precipitation and clogging, with water exiting only after 3 PV of injection. Clogging is influenced by the interplay of multiple forces, including gravity, inertia, electrostatic, and viscous forces (Zamani and Maini, 2009; Alamooti et al., 2022). Injection of a polymer solution containing 2 g/L of XG results in an unstable front progression, characterized by gravity-induced finger-like structures. Conversely, the injection of a 4 g/L XG solution yields a stable front advancement, possibly due to its unaffected viscosity.

To evaluate solution effectiveness, various quantification methods were employed, including relative density and pressure difference measurements at the column outlet. In Fig. 5a, the relative density of the outlet solution (ρ_{sol_out}), calculated as the ratio of the density of the outlet solution to the density of water (ρ_{water}), normalized by the initial injected solution density at the inlet (ρ_{sol_in}), denoted as (ρ_{sol_out}-ρ_{water})/(ρ_{sol_in}-ρ_{water}), is depicted at the column outlet for the delivery of the pyrite microparticles using pure water (solution 1) and xanthane biopolymer at 2 g/L and 4 g/L (solution 2). The injection of water alone (Water + Pyrite) proved ineffective in facilitating the successful transport of the pyrite microparticle powder. However, using xanthane biopolymer enhances significantly the delivery of the pyrite microparticles. The injection of xanthane and pyrite microparticle shows a gradually increasing relative density after column saturation. Specifically, at 1.1 PV, the relative density corresponds to 34 % and 47 % of the initial density for the xanthane concentration at 2 g/L and 4 g/L, respectively. Subsequently, after 3 PV, the relative density stabilizes at approximately 56 % and 66 % for the xanthane concentration at 2 g/L and 4 g/L, respectively. Therefore, using xanthane concentration at 4 g/L, enhances the delivery of the pyrite microparticle by around 25 %.

Fig. 5b illustrates the evolution of pressure difference in relation to the injected pore volume (PV). When considering the pressure dynamics for pure water (solution 1), the pressure difference at the onset of the injection is in the order of tens of Pascals. Due to the pyrite particle precipitation within the pores, the pressure gradually rises, reaching 0.7

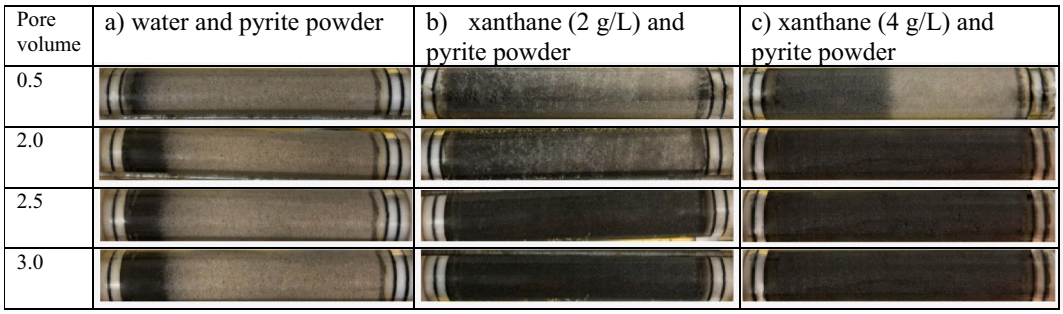

Fig. 4. Illustration of solution front propagation after 0.5, 2, 2.5, and 3 PV (Q = 3.48 mL/min) after injection of a) water and 24 g/L of FeS_2, b) polymer solution of 2 g/L and 24 g/L of FeS_2, and c) polymer solution of 4 g/L and 24 g/L of FeS_2.

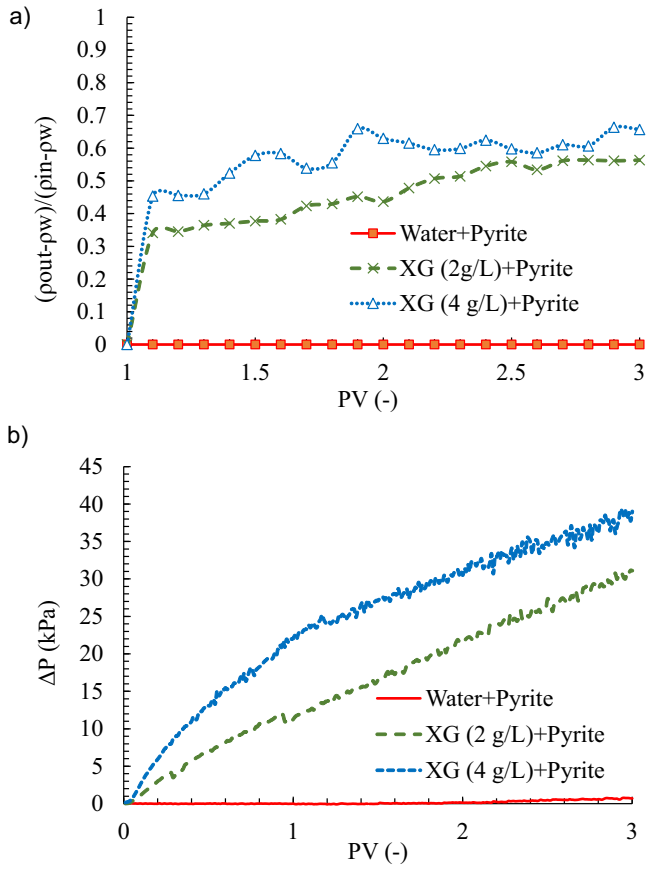

Fig. 5. Microparticle delivery capacity of pure water and xanthan biopolymer at 2 g/L and 4 g/L concentrations: a) Evolution of the relative density of effluent at the column outlet, and b) pressure difference as a function of injected pore volume (PV).

kPa after 3 PV. For biopolymer solutions, the onset of injection results in a gradual increase in the pressure difference, indicating pore filling and column resaturation with the polymer-based solution. However, after 1 PV, a steady-state fluid flow was not observed. Particle transport continued, and the pressure difference kept increasing, although at a slower rate. There is a noticeable reduction in the rate of pressure change for the xanthane solution at 4 g/L compared to the one at 2 g/L associated with pyrite powder (24 g/L). This suggests a improved particle transport for the xanthane solution at 4 g/L. The slope of the curve suggests a changing particle density, aligning with the relative density evolution observed at the column outlet, which consistently increases with injected PVs. According to Fig. 5b, the pressure difference and, consequently, the apparent viscosity of the xanthan biopolymer solution in porous media are approximately twice as high for the xanthan solution at 4 g/L compared to 2 g/L. As a result, the mobility ratio—defined as the ratio of the displacing fluid's mobility to the displaced fluid's mobility—is halved. This reduction in the mobility ratio decreases viscous fingering, leading to a more stable front propagation for the 4 g/L xanthan solution (Beteta et al., 2022; Davarzani et al., 2022). In addition, the increased viscosity hinders the settling of microparticles, offering resistance to gravitational forces and promoting uniform distribution. It is important to note that the apparent viscosity at the same shear rate can differ between porous media and polymer solutions measured with a rheometer. This discrepancy arises from particle deposition in the porous medium, which decreases its permeability (Omirbekov et al., 2023).

3.4.2. *Injectability of biopolymer-based sulfide solutions*

Various injection scenarios distinctly influence particle fronts and column saturation, with the 4 g/L XG solution demonstrating the most favorable outcomes. Consequently, injectability and stabilization tests were conducted in the packed column using the 4 g/L XG solution and two different sulfide reagents solutions (8, and 12). For solutions number 8 and 12, PIAX (100 g/L) and sodium thiosulfate (20 g/L) were added to the mixture of XG and pyrite powder, respectively, each containing 4 g/L of XG and 24 g/L of pyrite powder. Further details of the solutions are provided in Table 1.

We observed that, at a fixed pore volume (PV), the advancing front for solutions 2 (XG.F) and 8 (XG.PI.F) exhibited a slightly darker coloration, suggesting an enhanced efficiency in transporting pyrite particles. Subsequent to the injection of 1 PV, all columns achieved full saturation with polymer solutions, rendering them visually indistinguishable after 3 PVs.

In Fig. 6a, the relative density of the effluent at the column outlet is shown for the delivery of pyrite microparticles (24 g/L) using solutions 8 and 12, compared to the xanthan biopolymer at 4 g/L (solution 2). With the injection of solution 8 (XG + Pyrite+PIAX), we note stable and rapid growth in relative density immediately after column saturation, followed by erratic fluctuations after 2.5 PV. At 1.1 PV, the relative density registers at 28 %, and it progressively increases by 95 % at 2.5 PV. However, a temporary decline is observed at 2.8 PV, reducing the relative density to 88 %, before a resurgence to 88 % at 3 PV. This reflects a notable 60 % improvement in microparticle delivery from the initial post-saturation measurement. It is noteworthy that, the general pattern in relative density changes demonstrates an upward trend, suggesting an increased production of pyrite microparticles in the

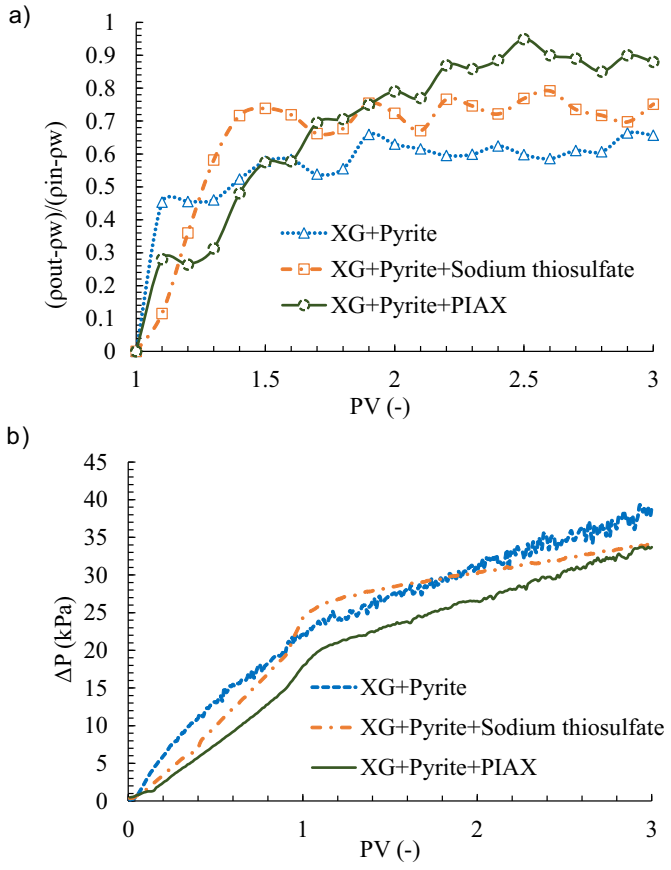

Fig. 6. Microparticle delivery capacity of biopolymer-based sulfide solutions 8 (xanthan 4 g/L + pyrite+PIAX) and 12 (xanthan 4 g/L + pyrite+sodium thiosulfate): a) Evolution of the relative density of effluent at the column outlet, and b) pressure difference as a function of injected pore volume (PV): a) Evolution of the relative density of solutions at the column outlet, and b) pressure difference as a function of injected pore volume (PV).

effluent. Nevertheless, fluctuations in this trend can be attributed to non-homogeneities in the distribution of the pyrite microparticles in the solutions during similar time steps.

Furthermore, the solution containing $Na_2S_2O_3$ (XG + Pyrite+Sodium thiosulfate) exhibits swift initial growth up to 1.5 PV, followed by gradual stabilization. Notably, at 1.1 PV, the relative density measures at 12 %, ultimately reaching 74 % (a 62 % increase) at 1.5 PV. A minor reduction of 2 % is observed at 2 PV, followed by a return to 75 % at 3 PV, indicating a 63 % increase from the initial post-saturation measurement. The solution containing PIAX demonstrates a higher density retention at 88 %, whereas the $Na_2S_2O_3$ solution exhibits a more expeditious enhancement in injectability with a relative density of 74 %. This enhanced capacity is due to its pyrite flotation behavior, which effectively prevents precipitation and clogging within the porous medium (Wang and Eric Forssberg, 1991; Yang et al., 2018). The incorporation of xanthan into reactive sulfide reagents significantly improves the transport of these reagents within pyrite microparticles in porous media. This intricate interaction between the rheological properties of the polymer solution and the dynamics between particles offers a comprehensive insight into the heightened stability of microparticles in viscous polymer solutions.

As shown in Fig. 6b, a similar trend is observed for the delivery of pyrite microparticles using both Solutions 8 and 12. A substantial increase in pressure precedes column saturation with the solution, followed by a more gradual pressure variation until the end of the injection. The introduction of xanthate PIAX (solution 8) results in a 23 % reduction in pressure difference compared to the delivery of particles using only the xanthane biopolymer. In the case of solution 12 (XG + Pyrite+sodium thiosolafate), the pressure gradient is not only less pronounced (8 % reduction) compared to the xanthane-only scenario (XG + Pyrite) but also exhibits a gradual growth curve after 1 PV. This plateau signifies more uniform and steady particle injection into the solution, which was partially anticipated due to the special properties of xanthate and thiosulfates (e.g., floating and lixiviation behaviors).

3.4.3. *Efficiency of Hg^0 stabilization in soil using biopolymer-based sulfide solutions*

Table 4 presents the initial and post-treatment effluent mercury concentrations for the Hg°-doped soil column using the selected solutions: Solution 8 (xanthan biopolymer + pyrite + PIAX) and Solution 12 (xanthan biopolymer + pyrite + sodium thiosulfate). The average initial mercury concentration in the effluent, following the injection of 3 pore volumes (PV) of water, was approximately 20 μg/L. This concentration decreased by approximately 14.4 times for Solution 8 and 4 times for Solution 12. After 3 days, the Hg effluent concentration further reduced to around 0.5 μg/L for Solution 8 and around 2.1 μg/L for Solution 12, indicating good stabilization of mercury within a short period. The kinetics of mercury stabilization to cinnabar were faster for Solution 8 compared to Solution 12. This observation is consistent with batch experiment results, where the silver color of the mercury droplet in contact with Solution 8 turned dark more rapidly, whereas Solution 12 caused a more gradual color change.

The mercury stabilization in these solutions is the result of the combined effect of sulfide solutions and the presence of pyrite microparticles. Both xanthate and sodium thiosulfate molecules contain two sulfur atoms each. However, xanthate has a higher potential for binding with mercury to form cinnabar (HgS) due to the more reactive nature of its sulfur atoms. Moreover, the rate and extent of mercury sulfide precipitation are influenced by parameters such as temperature, pH, and sodium thiosulfate concentration. Specifically, higher temperatures and thiosulfate concentrations, combined with lower pH levels, lead to an increased rate of mercury precipitation (Han et al., 2017a; Zhou and Dreisinger, 2017). Sodium thiosulfate ($Na_2S_2O_3$) readily reacts with mercury, forming stable complexes due to its strong affinity for the metal (Wang et al., 2012). Notably, $Na_2S_2O_3$ is a non-toxic compound, unlike Na_2S. The formation of HgS salt can be improved by adding a suitable amount of hydrochloric acid (HCl), which releases elemental sulfur that reacts with elemental mercury (Hg°) (Audeh, 1992). However, pyrite is effective in removing Hg° from aqueous solutions across a broad pH range (Brown et al., 1979) with longer reaction times (Svensson et al., 2006).

In our column experiments, evaluating the efficiency of the stabilization method required mobilizing the fluid around the polluted soil. This can enhance the leaching potential of sodium thiosulfate (Han et al., 2017b). In real scenarios, however, the polymer, being a highly viscous fluid, can block the flow around the contaminated zone. This blocking effect can enhance mercury stabilization and reduce or divert the downstream flow, thereby minimizing the dispersion of mercury in its dissolved phase within the groundwater.

Table 4
Initial and stabilized Hg^0 concentrations in Hg^0-doped sand-packed column using Solutions 8 (xanthan biopolymer + pyrite + PIAX) and 12 (xanthan biopolymer + pyrite + sodium thiosulfate). Dissolved Hg^0 concentration values are measured in the effluent. The values are the averages of 3 measurements related to the injection of 3 PV of water and 2 PV of polymer-based solutions.

Solutions	Averaged initial Hg^0 concentration in effluent (μg/L)	Averaged Hg^0 concentration in effluent just after treatment (μg/L)	Averaged Hg^0 concentration in effluent 3 days after treatment (μg/L)
8	20.2 ± 1.2	1.4 ± 0.6	0.5 ± 0.3
12	20.4 ± 1.5	5.1 ± 1.2	2.1 ± 0.4

4. Conclusions

The experimental investigation of reactive sulfide reagents and their delivery in porous media using xanthan gum biopolymer for in-situ mercury remediation has yielded valuable insights into environmental remediation strategies, particularly in the context of mercury stabilization. The xanthan polymer effectively maintained pyrite microparticles in suspension when viscosity was sufficiently high, ensuring their efficient transport through porous media. Introduction of pyrite microparticles and reactive sulfide solutions (sodium thiosulfate, sodium sulfide, and xanthate) into xanthan gum polymer systems resulted in a slight decrease in viscosity but did not significantly impact its shear-thinning behavior, which is crucial for bypassing soil heterogeneity and achieving uniform reagent distribution. Moreover, the introduction of xanthan polymer did not affect the ability of the sulfide solutions to stabilize elemental mercury, demonstrating their compatibility and synergistic effects. Sodium thiosulfate and organosulfur xanthate agents, notably PIAX, proved highly effective in reducing pressure gradients and increasing microparticle delivery efficiency, with PIAX exhibiting the most favorable performance. This is attributed to its unique floating behavior, which prevents precipitation and clogging within the porous medium. Furthermore, higher polymer concentrations (4 g/L of xanthan) exhibited enhanced delivery front stability, contributing to the precision and consistency of particle delivery. The elevated viscosity impedes the settling of microparticles, providing resistance against gravitational forces and ensuring uniform distribution. The combined effect of microparticle of pyrite, two sulfide-containing reagents (PIAX and sodium thiosulfate), and biopolymer allowed to stabilize the elemental mercury in a sand-packed column up to 97 % in the effluent. Xanthate is more effective than sodium thiosulfate in reacting with elemental mercury to form cinnabar (HgS). This is because xanthates contain sulfur in a form that readily interacts with mercury to produce the desired sulfide compound. Furthermore, xanthate renders the pyrite microparticles hydrophobic, facilitating their entry into the mercury droplets. This results in the formation of a black paste that stabilizes not only the surface but also the elemental mercury droplet throughout its depth. Pyrite, being the most prevalent metal sulfide in nature, is widely accessible and cost-effective. It can be prepared as a powder and combined with the xanthane biopolymer and reactive reagent presented in

this study to adsorb and stabilize elemental mercury effectively. The selection of the reagent solution will depend on the soil's characteristics such as pH and composition, as well as considerations of reagent availability and cost-effectiveness. These products can be prepared in aqueous solutions and injected directly into contaminated soil zones using injection wells or boreholes. These findings provide strong evidence for the potential of xanthan gum and xanthate in in-situ mercury remediation, offering promising solutions for addressing environmental challenges.

CRediT authorship contribution statement

Dorian Davarzani: Writing – review & editing, Writing – original draft, Supervision, Resources, Project administration, Methodology, Funding acquisition, Conceptualization. **Zeinab Derikvand:** Writing – original draft, Validation, Formal analysis. **Stéphanie Betelu:** Writing – review & editing, Validation, Software, Investigation. **Stéfan Colombano:** Resources, Project administration. **Marcio Nascimento:** Writing – original draft, Visualization, Data curation, Conceptualization. **Ioannis Ignatiadis:** Investigation, Validation, Writing – review & editing. **Daniel Hubé:** Writing – review & editing, Conceptualization.

Declaration of competing interest

The authors declare that they have no known competing financial interests or personal relationships that could have appeared to influence the work reported in this paper.

Data availability

Data will be made available on request.

Acknowledgments

This study was performed as part of the research and development M4-POUSSE project. The authors would like to thank BRGM DRPC and DEPA for providing the project's financial support. We gratefully acknowledge the financial support provided to the PIVOTS project by the “Région Centre – Val de Loire” and the European Regional Development Fund.

References

Abeysinghe, K.S., Qiu, G., Goodale, E., Anderson, C.W.N., Bishop, K., Evers, D.C., Goodale, M.W., Hintelmann, H., Liu, S., Mammides, C., 2017. Mercury flow through an Asian rice-based food web. Environ. Pollut. 229, 219–228.

Alamooti, A., Colombano, S., Omirbekov, S., Ahmadi, A., Lion, F., Davarzani, H., 2022. Influence of the injection of densified polymer suspension on the efficiency of DNAPL displacement in contaminated saturated soils. J. Hazard. Mater. 440, 129702. https://www.sciencedirect.com/science/article/pii/S0304389422014959.

Audeh, C.A., 1992. Fixation of elemental mercury present in spent molecular sieve desiccant for disposal. In: U.S. Patent 5,173,286.

Beteta, A., Sorbie, K.S., McIver, K., Johnson, G., Gasimov, R., van Zeil, W., 2022. The role of immiscible fingering on the mechanism of secondary and tertiary polymer flooding of viscous oil. Transp. Porous Media 143 (2), 343–372. https://doi.org/10.1007/s11242-022-01774-8.

Bower, J., Savage, K.S., Weinman, B., Barnett, M.O., Hamilton, W.P., Harper, W.F., 2008. Immobilization of mercury by pyrite (FeS2). Environ. Pollut. 156, 504–514.

Brown, J.R., Bancroft, G.M., Fyfe, W.S., McLean, R.A.N., 1979. Mercury removal from water by iron sulfide minerals. An electron spectroscopy for chemical analysis (esca) study. Environ. Sci. Technol. 13 (9), 1142–1144. https://doi.org/10.1021/es60157a013.

Chen, Z.Y., Zhang, H.Z., 2012. Research on extract remediation technology of mercury-contaminated soils. Earth Sci. Front. 19, 230–235.

Davarzani, H., Philippe, N., Cochennec, M., Colombano, S., Dierick, M., Ataie-Ashtiani, B., Klein, P.-Y., Marcoux, M., 2022. Numerical simulations of high viscosity DNAPL recovery in highly permeable porous media under isothermal and non-isothermal conditions. J. Contam. Hydrol. 251, 104073. https://www.sciencedirect.com/science/article/pii/S0169772222001218.

Duan, Y., Han, D.S., Batchelor, B., Abdel-Wahab, A., 2016. Synthesis, characterization, and application of pyrite for removal of mercury. Colloid. Surf. A Physicochem. Eng. Asp. 490, 326–335.

Gao, F., Song, Y., Li, Z., Xiong, F., Chen, L., Zhang, X., Chen, Z., Moortgat, J., 2018. Quantitative characterization of pore connectivity using NMR and MIP: a case study of the Wangyinpu and Guanyintang shales in the Xiuwu basin, Southern China. Int. J. Coal Geol. 197, 53–65.

Gong, Y., Huang, Y., Wang, M., Liu, F., Zhang, T., 2019. Application of iron-based materials for remediation of mercury in water and soil. Bull. Environ. Contam. Toxicol. 102, 721–729.

Hagemann, S.. Technologies for the stabilization of elemental mercury and mercury-containing wastes. Gesellschaft für Anlagen-und Reaktorsicherheit (GRS, GRS Report 252). https://wedocs.unep.org/bitstream/handle/20.500.11822/11456/grs_252_stabmerc.pdf?sequence=1&isAllowed=y.

Han, C., Wang, H., Xie, F., Wang, W., Zhang, T., Dreisinger, D., 2017a. Feasibility study on the use of thiosulfate to remediate mercury-contaminated soil. Environ. Technol. 40 (7), 813–821. https://doi.org/10.1080/09593330.2017.1408693.

Han, C., Wang, W., Xie, F., Zhang, T., 2017b. Mechanism and kinetics of mercuric sulfide leaching with cuprous-thiosulfate solutions. Sep. Purif. Technol. 177, 223–232. https://www.sciencedirect.com/science/article/pii/S1383586616303070.

Han, Y.-S., Kim, S.-H., Chon, C.-M., Kwon, S., Kim, J.G., Choi, H.W., Ahn, J.S., 2020. Effect of FeS on mercury behavior in mercury-contaminated stream sediment: a case study of Pohang Gumu Creek in South Korea. J. Hazard. Mater. 393, 122373.

Han, P., Xie, J., Qin, X., Yang, X., Zhao, Y., 2022. Experimental study on in situ remediation of Cr (VI) contaminated groundwater by sulfidated micron zero valent iron stabilized with xanthan gum. Sci. Total Environ. 828, 154422.

Ko, M.-S., Jeon, Y.-J., Kim, K.-W., 2022. Novel application of xanthan gum-based biopolymer for heavy metal immobilization in soil. J. Environ. Chem. Eng. 10, 108240.

Li, C., Zhou, K., Qin, W., Tian, C., Qi, M., Yan, X., Han, W., 2019. A review on heavy metals contamination in soil: effects, sources, and remediation techniques. Soil Sediment Contam. An Int. J. 28, 380–394.

Liu, D., Ren, L., Wen, C., Dong, J., 2018. Investigation of the compatibility of xanthan gum (XG) and calcium polysulfide and the rheological properties of XG solutions. Environ. Technol. 39, 607–615.

Liu, W., Bai, J., Chi, Z., Ren, L., Dong, J., 2021a. An in-situ reactive zone with xanthan gum modified reduced graphene oxide supported nanoscale zero-valent iron (XG-nZVI/rGO) for remediation of Cr (VI)-polluted aquifer: dynamic evolutions of Cr (VI) and environmental variables. J. Environ. Chem. Eng. 9, 104987.

Liu, S., Wang, X., Guo, G., Yan, Z., 2021b. Status and environmental management of soil mercury pollution in China: a review. J. Environ. Manag. 277, 111442.

Lyu, H., Gong, Y., Tang, J., Huang, Y., Wang, Q., 2016. Immobilization of heavy metals in electroplating sludge by biochar and iron sulfide. Environ. Sci. Pollut. Res. 23, 14472–14488.

Mahbub, K.R., Bahar, M.M., Labbate, M., Krishnan, K., Andrews, S., Naidu, R., Megharaj, M., 2017. Bioremediation of mercury: not properly exploited in contaminated soils! Appl. Microbiol. Biotechnol. 101, 963–976.

Nsengiyumva, E.M., Alexandridis, P., 2022. Xanthan gum in aqueous solutions: fundamentals and applications. Int. J. Biol. Macromol. 216, 583–604.

Omirbekov, S., Colombano, S., Alamooti, A., Batikh, A., Cochennec, M., Amanbek, Y., Ahmadi-Senichault, A., Davarzani, H., 2023. Experimental study of dnapl displacement by a new densified polymer solution and upscaling problems of aqueous polymer flow in porous media. J. Contam. Hydrol. 252, 104120. https://www.sciencedirect.com/science/article/pii/S0169772222001681.

Patel, J., Maji, B., Moorthy, N.S.H.N., Maiti, S., 2020. Xanthan gum derivatives: review of synthesis, properties and diverse applications. RSC Adv. 10, 27103–27136.

Peng, Z., Xiong, C., Wang, W., Tan, F., Wang, X., Qiao, X., Wong, P.K., 2018. Hydrophobic modification of nanoscale zero-valent iron with excellent stability and floatability for efficient removal of floating oil on water. Chemosphere 201, 110–118. https://www.sciencedirect.com/science/article/pii/S0045653518303618.

Rao, S., Finch, J., 2003. Base metal oxide flotation using long chain xanthates. Int. J. Miner. Process. 69 (1), 251–258. https://www.sciencedirect.com/science/article/pii/S0301751602001308.

Ray, A.B., Selvakumar, A., 2000. Laboratory studies on the remediation of mercury contaminated soils. Remediat. J. 10, 49–56.

Rezaeiakmal, F., Parsaei, R., Shafiabadi, A., Rezaei, A., 2022. Insights into the flow behaviour of the pre-generated polymer enhanced foam in heterogeneous porous media during tertiary oil recovery: effect of gravitational forces. J. Pet. Sci. Eng. 213, 110385 https://doi.org/10.1016/j.petrol.2022.110385.

Rodríguez, O., Padilla, I., Tayibi, H., López-Delgado, A., 2012. Concerns on liquid mercury and mercury-containing wastes: a review of the treatment technologies for the safe storage. J. Environ. Manag. 101, 197–205.

Shabir, R., Li, Y., Megharaj, M., Chen, C., 2023. Biopolymer as an additive for effective biochar-based rhizobial inoculant. Sci. Total Environ. 912, 169263 https://doi.org/10.1016/j.scitotenv.2023.169263.

Sierra, C., Menéndez-Aguado, J.M., Afif, E., Carrero, M., Gallego, J.R., 2011. Feasibility study on the use of soil washing to remediate the As–Hg contamination at an ancient mining and metallurgy area. J. Hazard. Mater. 196, 93–100.

Skyllberg, U., Persson, A., Tjerngren, I., Kronberg, R.-M., Drott, A., Meili, M., Björn, E., 2021. Chemical speciation of mercury, sulfur and iron in a dystrophic boreal lake sediment, as controlled by the formation of mackinawite and framboidal pyrite. Geochim. Cosmochim. Acta 294, 106–125.

Sun, Y., Lv, D., Zhou, J., Zhou, X., Lou, Z., Baig, S.A., Xu, X., 2017. Adsorption of mercury (II) from aqueous solutions using FeS and pyrite: a comparative study. Chemosphere 185, 452–461.

Svensson, M., Allard, B., Düker, A., 2006. Formation of HgS—mixing HgO or elemental Hg with S, FeS or FeS2, Science of The Total Environment 368(1), 418–423. In: Selected Papers from the 7th International Conference on Mercury as a Global

Pollutant, Ljubljana, Slovenia June 27 - July 2, 2004. https://www.sciencedirect.com/science/article/pii/S0048969705006625.
Tungittiplakorn, W., Cohen, C., Lion, L.W., 2005. Engineered polymeric nanoparticles for bioremediation of hydrophobic contaminants. Environ. Sci. Technol. 39, 1354–1358.
Ukaogo, P.O., Ewuzie, U., Onwuka, C.V., 2020. Environmental pollution: causes, effects, and the remedies. In: Microorganisms for Sustainable Environment and Health. Elsevier, pp. 419–429.
Wang, X.-H., Eric Forssberg, K., 1991. Mechanisms of pyrite flotation with xanthates. Int. J. Miner. Process. 33 (1), 275–290. Flotation of sulphide minerals 1990. https://www.sciencedirect.com/science/article/pii/030175169190058Q.
Wang, J., Feng, X., Anderson, C.W.N., Wang, H., Zheng, L., Hu, T., 2012. Implications of mercury speciation in thiosulfate treated plants. Environ. Sci. Technol. 46 (10), 5361–5368. https://doi.org/10.1021/es204331a.
Wang, L., Hou, D., Cao, Y., Ok, Y.S., Tack, F.M.G., Rinklebe, J., O'Connor, D., 2020. Remediation of mercury contaminated soil, water, and air: a review of emerging materials and innovative technologies. Environ. Int. 134, 105281.
Yang, X., Albijanic, B., Liu, G., Zhou, Y., 2018. Structure–activity relationship of xanthates with different hydrophobic groups in the flotation of pyrite. Miner. Eng. 125, 155–164. https://www.sciencedirect.com/science/article/pii/S0892687518302590.
Ying, Y., Zhou, Q., 2005. A review on chemical remediation technology of contaminated soils. Tech. Equip. Environ. Pollut. Control 6, 1–7.
Zamani, A., Maini, B., 2009. Flow of dispersed particles through porous media — deep bed filtration. J. Pet. Sci. Eng. 69 (1), 71–88. https://www.sciencedirect.com/science/article/pii/S0920410509001430.
Zhao, C., Liu, G., Tan, Q., Gao, M., Chen, G., Huang, X., Xu, X., Li, L., Wang, J., Zhang, Y., Xu, D., 2023. Polysaccharide-based biopolymer hydrogels for heavy metal detection and adsorption. J. Adv. Res. 44, 53–70. https://www.sciencedirect.com/science/article/pii/S2090123222001011.
Zhou, Z., Dreisinger, D., 2017. An investigation of mercury stabilization techniques through hypochlorite leaching and thiosulfate/selenosulfate precipitation. Hydrometallurgy 169, 468–477. https://www.sciencedirect.com/science/article/pii/S0304386X16302079.